Erzincan Üniversitesi
Fen Bilimleri Enstitüsü Dergisi
2023, 16(1), 239-257
ISSN: 1307-9085, e-ISSN: 2149-4584
Araştırma Makalesi

Erzincan University
Journal of Science and Technology
2023, 16(1), 239-257
DOI: 10.18185/erzifbed.1247007
Research Article

Electrochemical Behavior of $CoO/Ag_2O/TiO_2$ Ceramic and Composite Coated Selective Laser Manufactured 316L Stainless Steel

Tuba YETİM[1*]

[1]Erzurum Technical University, Faculty of Engineering and Architecture, Department of Chemical Engineering, Erzurum, Turkey

Received:03/02/2023, **Revised:** 27/02/2023, **Accepted:** 28/02/2023, **Published:** 30/03/2023

Abstract

In order to improve the corrosion resistance of 316L stainless steel manufactured by Selective Laser Melting (SLM) additive manufacturing, Ag_2O, CoO, and TiO_2 separately and $Ag_2O/CoO/TiO_2$ composite ceramic films were coated on the 316L surface by a sol-gel dip coating method. The structural properties of the uncoated and coated samples were characterized by XRD and SEM. The corrosion resistance for all samples was evaluated by potentiodynamic polarization and electrochemical impedance spectroscopy (EIS) tests in the simulated saliva fluid (SSF). According to the experimental results, quite dense, non-colonic, non-porous, compact, and between 30-40 μm thicknesses ceramic oxide films were formed successfully on the 316L sample surface. Also, all ceramic films increased the corrosion resistance of the 316L surface. The most corrosion-resistant surface was obtained at the $Ag_2O/CoO/TiO_2$ composite ceramic film-coated 316L surface.

Keywords: Additive manufacturing (SLM), 316L stainless steel, ceramic coating films, sol-gel dip coating, corrosion

$CoO/Ag_2O/TiO_2$ Seramik ve Kompozit ile Kaplanan Seçici Lazer ile Üretilmiş 316L Paslanmaz Çeliğin Elektrokimyasal Davranışı

Öz

Seçici lazer ergitme eklemeli üretim yöntemi ile üretilmiş 316L paslanmaz çeliğinin korozyon direncini artırmak için ayrı ayrı Ag_2O, CoO, ve TiO_2 ve $Ag_2O/CoO/TiO_2$ kompozit seramik film 316L yüzeyine sol-jel dip kaplama metodu ile kaplandı. Kaplanmış ve kaplanmamış numunelerin yapısal özellikleri XRD ve SEM ile karakterize edildi. Numunelerin tamamının korozyon direnci simüle edilmiş yapay tükürük sıvısı içerisinde potansiyodinamik polarizasyon ve elektrokimyasal empedans spektroskopi (EIS) testleri değerlendirildi. Test sonuçlarına göre, oldukça yoğun, kolonsal ve porlu olmayan, kompakt ve 30-40 μm kalınlığında seramik oksit filmler 316L yüzeyinde oluşturuldu. Ayrıca bütün seramik filmler 316L yüzeyinin korozyon direncini artırdı. En yüksek korozyon dirençli yüzey $Ag_2O/CoO/TiO_2$ kompozit seramik film kaplı 316L yüzeyinde elde edildi.

Anahtar Kelimeler: Eklemeli imalat (SLM), 316L paslanmaz çelik, seramik kaplamalı filmler, sol-jel daldırmalı kaplama, korozyon

*Corresponding Author: tuba.yetim@erzurum.edu.tr
Tuba YETİM, https://orcid.org/0000-0002-6237-6412

1. Introduction

Recently, the additive manufacturing method has become a very remarkable and popular production method used in the production of parts in many fields such as healthcare, aerospace, automobile manufacturing, and medical materials [1-5]. Additive manufacturing (AM) technology is based on the layer-by-layer deposition of materials in three-dimensional form. In this way, complex geometries can be produced at a low-cost [1, 6-11]. Among various AM technologies, selective laser melting (SLM) has been widely preferred in manufacturing used to produce Co-Cr-Mo, stainless steel, titanium, and its alloys [12-15]. In the SLM mechanism, a powder layer with a defined thickness is deposited on a movable base plate. Then, a precise laser beam scans the powder bed according to the slice data of a CAD model. Powder particles are melted quickly by the laser beam completely and the melt quickly solidifies to form a solid layer. After this, the piston moves down a defined distance, and the next powder layer is deposited. This process is repeated layer by layer until the production is completed. Finally, the non-sintered powder is removed, and the product is completed. The SLM factors such as the powder particle size and distribution, the thickness of the deposited powder layer, beam power and thickness, scanning rate, and distance between scanning points affect the quality of the final products [16-23].

316L stainless steel is widely used as biomaterials in the medical field because of its easy and low-cost manufacturing, good loading capacity, and excellent mechanical property [7,24-26]. However, it is difficult for 316L stainless steel to form a real chemical bond with human bone tissue due to its low biocompatibility, low bioactivity, and high modulus of elasticity [27-28]. On the other hand, the corrosion and wear resistance of 316L stainless steel is poor in vivo environment. It has been reported in some studies that the Cr^{3+} and Cr^{5+} cations can be released from the 316L stainless steel, and they diffuse to surrounding tissues, causing inflammation and necrosis of these tissues. This event ultimately leads to implantation failure due to corrosion and wear [27,7,29-30]. Therefore, surface treatments are applied to the 316L to overcome these problems. The surface modification technology of steel mainly includes thermal chemical reaction spraying, sol−gel, slurry, PVD, CVD, and plasma spray processes [27,31−33]. For surface treatment ceramic coatings are widely and effectively used to increase surface strength and corrosion resistance. Also, the sol-gel process is preferred for the production of protective ceramic films on the substrate. Due to its advantageous properties such as low equipment and production costs, controllable composition, low process temperature, well homogeneity, and no size limit advantage properties of sol-gel process, it is widely preferred use [34-37].

In this study, the 316L samples were produced by the SLM method. For surface treatment, the 316L samples were coated with Ag_2O, CoO, and TiO_2 separately and $Ag_2O/CoO/TiO_2$ composite ceramic structures by the sol-gel dip-coating method. After the coating process, the structural and corrosion behavior of the coated and uncoated samples were investigated. The aim of this study is to form the various ceramic structures on the SLM-manufactured 316L stainless steel (316L) and to increase the corrosion resistance of the 316L surface.

2. Materials and Methods

316L stainless steel (316L) specimens with the dimensions of 20 × 20 × 4 mm were produced by utilizing Laser Powder Bed Fusion additive manufacturing. The chemical composition of 316L powder is given in Table 1. Certified CL 20 ES 316L stainless steel powder was used in this study. The used powder was produced for medical purposes and it was indicated by the manufacturer that the average powder size was approximately 25 μm. Additive manufacturing operations were carried out using the MLab Cusing R Machine from Concept Laser, with 100W Ytterbium (Yb) fiber laser. Straight-line laser scans were utilized to melt each layer. The 316L specimen was produced in a nitrogen environment. The production parameters recipe for 316L stainless steel, which was determined and recommended by the manufacturer of the device, was used in the following values by keeping the parameters constant. The process parameters for SLM were; a laser power of 40 W, a scanning speed of 400 mm/s, parallel scanning of 100 μm, a layer thickness of 25 μm, and a scan rotation of 90°. Before the dip-coating process for surface treatment, the oxide layer existing on the surface of the 316L specimens was eliminated via polishing by SiC emery paper (80 to 1000 mesh grit). At the end of this preparation, specimens were polished with 0.3 μm alumina. Afterward, the specimens were cleaned ultrasonically in an ethanol bath. For the dip-coating by sol-gel process, the necessary ceramic coating solutions were prepared by using the silver nitrate ($AgNO_3$), cobalt II chloride hexahydrate ($CoCl_2.6H_2O$), titanium IV isopropoxide (TTIP), hydrazine hydrate ($N_2H_4.H_2O$), ammonium hydroxide (NH_4OH) and hydrochloric acid (HCl) chemicals obtained from Sigma-Aldrich and Merck and used any purification. All the ceramic film coating solutions were prepared at 0.5M of concentration. Each ceramic film coating solution was prepared as follows:

- Ag_2O ceramic film coating solution; The required mass amount of silver nitrate for 0.5 molars is dissolved in 100 milliliters of pure water. Ammonium hydroxide is added to the solution drop by drop until the pH reaches 12. This solution is mixed for about 2 hours with a magnetic stirrer. The solution is aged for 24 hours.
- CoO ceramic film coating solution; The required mass amount of cobalt II chloride hexahydrate for 0.5 molars is dissolved in 100 milliliters of pure water. 5 ml of hydrazine hydrate and the ammonium hydroxide is added to the solution drop by drop until the pH reaches 10. This solution is mixed for about 2 hours with a magnetic stirrer. The solution is aged for 24 hours.
- TiO_2 ceramic film coating solution; 74.7 ml pure water, and 8.8 ml HCl are mixed on a heated magnetic stirrer. When the temperature reaches 70°C 15.5 ml TTIP is added to the solution drop by drop. This solution is mixed for about 2 hours with a magnetic stirrer at that temperature. Then the solution is aged at room temperature for 24 hours.
- $Ag_2O/CoO/TiO_2$ composite ceramic film coating solution; For 0.5 molars of the composite solution, the required mass amount of silver nitrate, cobalt II chloride hexahydrate, and TTIP are used as equal amounts. They are dissolved in 100 milliliters of pure water. 5 ml of hydrazine hydrate and ammonium hydroxide is added to the solution drop by drop until the pH reaches 12. This solution is mixed for about 2 hours with a magnetic stirrer. The solution is aged for 24 hours.

After the preparation of coating solutions, the coating process was carried out by dip-coating method as follows. 316L substrate samples were immersed into the sol-gel solution at a constant speed of 10 $cm.min^{-1}$. The samples were kept in solution for 10 minutes. Then, they were removed from the solution at the same speed, and they were left to remove the excess solution from the sample for about 10 minutes. The dipping and removing processes were carried out in a vertical direction by the dip-coating device at room temperature. After that, they were dried in an oven at 100°C for 10 minutes. This process circle was repeated 3 times for a sample. Finally, the calcination was applied to the films on the coated sample surface with the thermal heat treatment furnace and it was open to the atmosphere. The calcination process was applied for 2 hours after the temperature reached the 500°C. This process steps were repeated for all coating samples. After the coating process, the samples were analyzed for determining the film structure and the electrochemical behavior of the samples.

Table 1. Chemical Composition (%W) of 316L Stainless Steel Powder

Cr	Ni	Mo	P	Mn	Si	C	S	Fe
16.5-18.5	10-13	2-2.5	0-0.045	0-2	0-1	0-0.03	0-0.03	Balanced

To analyze the structural properties, XRD measurements were carried out by using an XRD-GNR-Explorer operated at 40 kV and 30 mA Cu Kα1 ((λ=1.540 Å) source diffractometer with 2θ scale from 10º to 100º. Cross-section and corroded surface images were also examined by Scanning electron microscope (SEM FEI-Quanta 250). Corrosion properties of untreated and coated samples were performed by a Gamry Series G750 potentiostat/galvanostat. For determining the corrosion behavior of all samples, simulated saliva fluid (SSF) was prepared at pH=6.5 to use in potentiodynamic polarization and Electrochemical Impedance Spectroscopy (EIS) tests. All corrosion measurements were conducted in simulated saliva fluid (SSF). The chemical composition of the SSF solution is shown in Table 2 [38-39]. Moreover, corrosion test results and data analyses were evaluated via Gamry Echem Analyst software. The electrochemical measurements were applied according to the three-compartment cell containing reference electrode (Ag/AgCl), counter electrode (graphite), and working electrode in 50 ml SSF solutions where 0.502 cm^2 surface area was exposed to corrosion. Open circuit potential (OCP), potentiodynamic polarization, and electrochemical impedance spectroscopy (EIS) measurements were conducted in all samples.

Table 2. Chemical Composition of Simulated Saliva Fluid (SSF)

Composition	Used amount (g/l)
Potassium chloride	0.720
Calcium chloride dihydrate	0.220
Sodium chloride	0.600
Potassium phosphate monobasic	0.680
Sodium phosphate dibasic	0.866 (dodecahydrate)
Potassium bicarbonate	1.500
Potassium thiocyanate	0.060
Citric Acid	0.030

3. Results and Discussion

3.1. Microstructural and morphological examinations

XRD pattern of untreated 316L, separately cobalt oxide, silver oxide, titanium oxide, and composite CoO/Ag_2O/TiO_2 coated samples are given in Figure 1. As expected, 316L stainless steel exhibited γ-austenite peaks with a face-centered-cubic (FCC) structure. It was observed that the leading peaks of γ-austenite were (111) and (200). In the case of the coated samples, XRD analysis showed that different oxide coating processes occurred successfully on the substrate. Although austenite peaks are still present from the substrate, it was seen that different metal oxides were formed according to the oxide coating type. It was determined that the rutile type TiO_2 structure was diffracted from the TiO_2 coatings. On the other hand, it is seen that CoO peaks are reflected in cobalt oxide coatings and also Ag_2O peaks in silver oxide coatings, as expected. In the triple composite coating, although formations of all three metal oxides were observed, it was determined that the dominant phase was TiO_2 because of its lower activation than others.

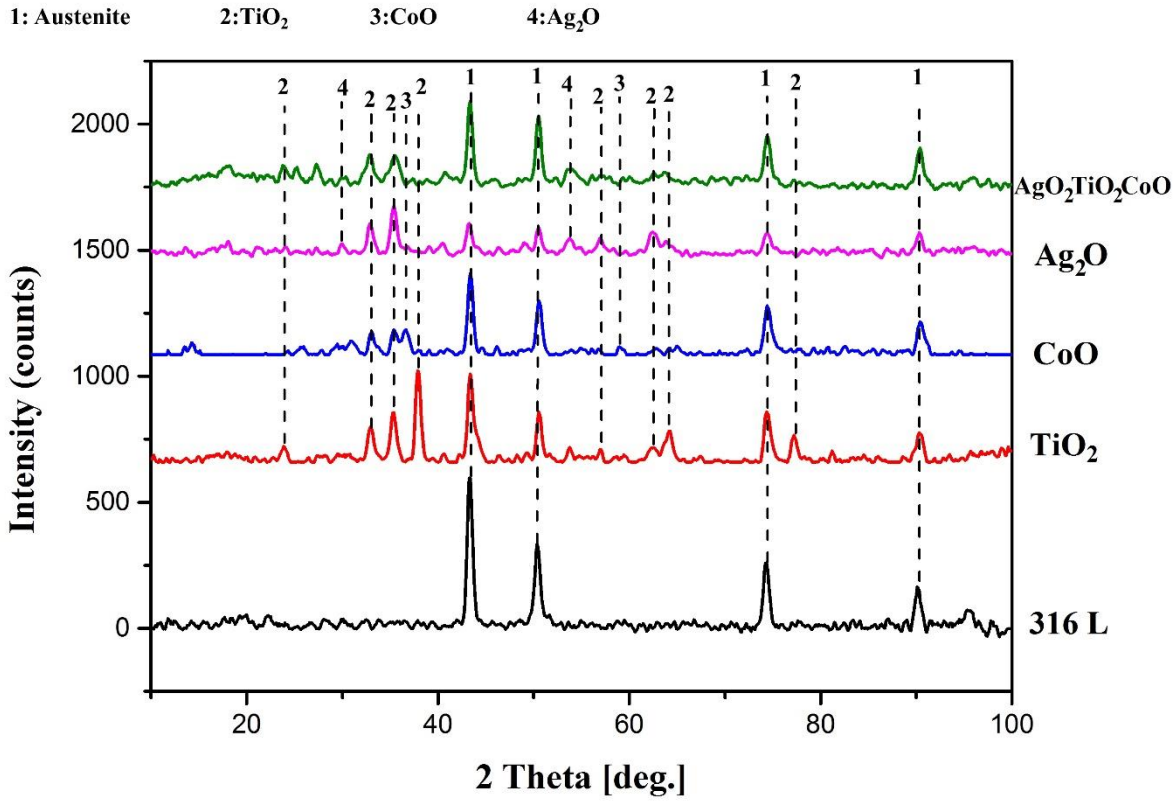

Figure 1. XRD pattern of untreated 316L, Ag_2O, CoO, TiO_2 and composite Ag_2O/CoO/TiO_2 coated samples

Figure 2 shows the cross-section SEM images of CoO, Ag_2O, TiO_2, and composite Ag_2O/CoO/TiO_2 coated samples. Similar morphological features were observed in all coated samples. As a whole, it was seen that the films were quite dense, non-colonic, non-porous, and

compact, and a very thin and rough texture was formed on the surface of these films (Figure 2a-d). All these metal oxide film thicknesses values were measured between 30-40 μm.

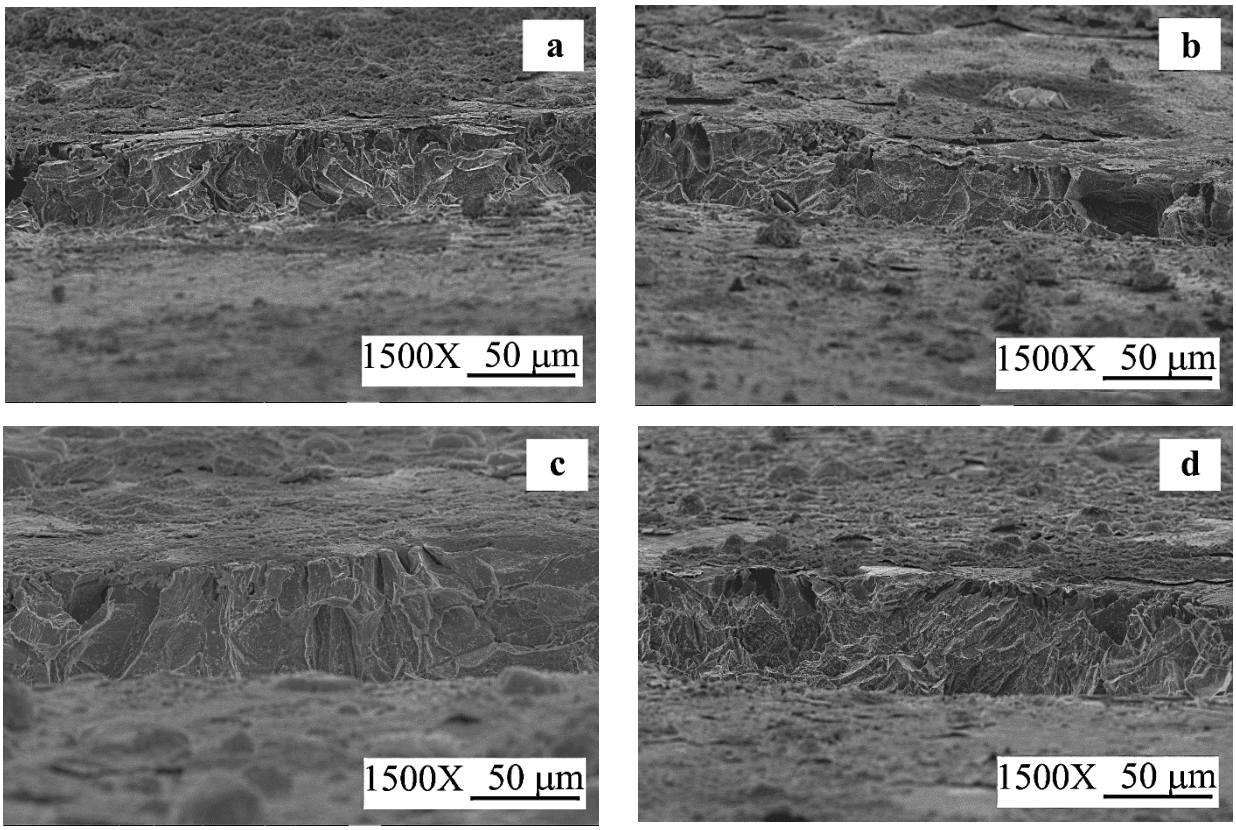

Figure 2. Cross-section SEM images of a) CoO, b) Ag_2O, c) TiO_2 and d) composite $Ag_2O/CoO/TiO_2$ coated samples

3.2. Electrochemical Behavior

Before the potentiodynamic and electrochemical impedance spectroscopy (EIS) tests, the open circuit potential (OCP) values were measured for determining the passivation behavior of both untreated and all ceramic-coated samples. Simulated saliva fluid was used during all electrochemical behavior-determining experiments. The sample to be analyzed was immersed in the simulated saliva fluid until obtaining a steady-state open circuit potential (OCP). It was repeated for all samples. This test was applied for 5000s and before this value, the potential difference was stable and reached a steady-state form for all samples. After equilibration, polarization was started by 0.5 mVs^{-1} rate from the potential range of – 1.0 to +2.0 V vs OCP. When the anodic potentials reached over 2.0 V for all samples, the scanning processes were stopped. EIS measurements were carried out using AC signals at the OCP values of samples in the frequency range of 100000–0.01 Hz. The surface area of the corroded surfaces was 0.502 cm^2 and all data have been normalized according to the surface area.

The comparative potentiodynamic polarization curves (PDS) of the untreated and ceramic-coated samples and also some important corrosion parameters calculated from these curves are presented in Figure 3 and Table 3, respectively. From Figure 3, it was seen that the current remained constant as the potential increased at a zone which was called the passivation region.

Because of the forming a of passive oxide layer on the sample surface, it was encountered by this behavior. As a result of redox reactions in the corrosion mechanism, the metal immigrated into the electrolyte as cations. Then they reduced according to the redox reactions and the products collapsed on the sample surface. So that a passive layer forms on the anodic zone. This passive layer prevented the flow of current hence, the corrosion was prevented or slowed down. It was observed that as the increasing potential value, the current value increased. Also, this passive layer was broken and corrosion began again or continues rapidly after a period of time. This case was seen in the transpassive zone, and it occurred after the passive zone in Figure 3. Also, the protective efficiency P (%) of the samples can be estimated by Eq. (1):

$$P_i(\%) = [1 - (i_{corr}/i^0_{corr})] \times 100$$

where I_{corr} and I^0_{corr} are the corrosion current densities of the coated samples and substrate, respectively. The protective efficiency values of the Ag_2O, CoO, TiO_2, and $Ag_2O/CoO/TiO_2$ composite ceramic coatings were approximately 24.4%, 42.9%, 64.6%, and 88.9% respectively.

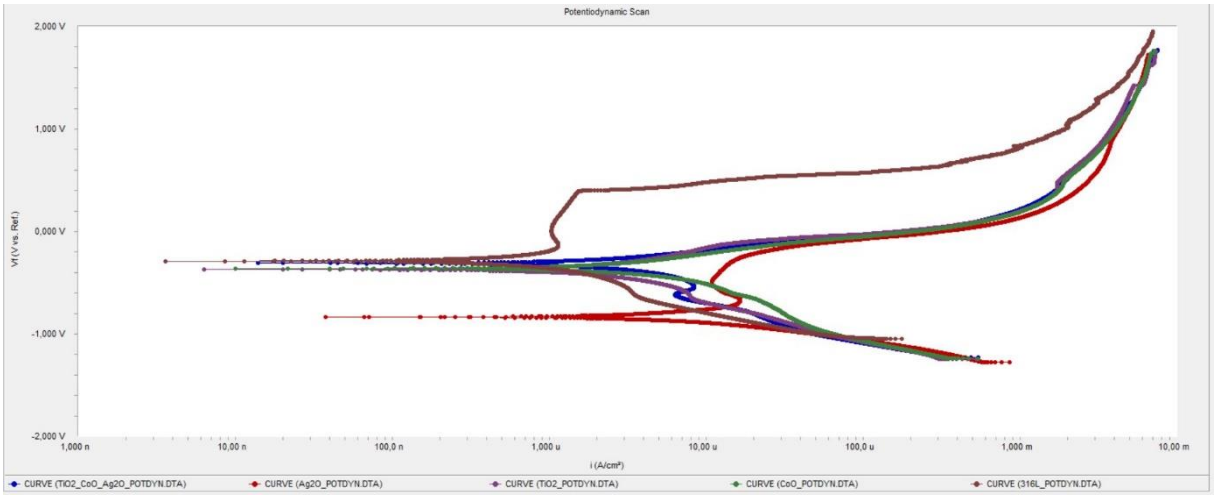

Figure 3. Potentiodynamic polarization curves of uncoated and ceramic-coated samples

Table 3. Corrosion values of all samples

	Icorr (mA/cm^2)	**Ecorr (mV)**	**Corr.Rate (mpy)**
316L	8.99×10^{-3}	-288	5.665
Ag_2O	6.80×10^{-3}	-835	4.283
CoO	5.13×10^{-3}	-360	3.230
TiO_2	3.18×10^{-3}	-372	2.007
$Ag_2O/CoO/TiO_2$	1.00×10^{-3}	-310	0.632

From the corrosion test results, it can be seen that the 316L, the untreated sample, had the most corrosion rate among all the analyzed samples. Also, its current density (I_{corr}) was the biggest value among the other samples, as expected. It means that the untreated and unprotected sample draws a large current or in other words, a large amount of current can pass into the untreated

sample. Thus the necessary electrons would be provided for the corrosion to continue. So the sample is heavily exposed to the corrosion process and the corrosion rate is determined as high, as seen in Table 3.

In Table 3, the corrosion rate and current density of untreated 316L are higher than the other samples, which means that the resistance is low. This is an expected result. However, the high Ecorr value of 316L is not an expected result according to the above results. This unexpected result can be attributed to the production of 316L with SLM. It can be explained as in the following: It is known that the materials are produced layer by layer in selective additive manufacturing by laser melting with material powders. Although this method widens the range of geometry diversity of the materials to be produced and has many benefits, there are still many unresolved research questions, such as those involving inhomogeneity in material deposition or during the layer-by-layer fabrication of components, which leads to undesirable micro-structures and excessive surface roughness [40] also, it is thought that the defects that may occur at the junction points of the layers without being aware of it during the production. Also these defects cause the formation of short circuits at the junction points of the layers can be thought as welding points. While there is resistance in other regions, the current can easily pass due to the much lower resistance in these junction points, so that the corrosion rate increases. It is known that in the short circuits systems higher current passes on the lower resistance at a constant potential source, usually. But in this corrosion analysis system the potential range was -1.0 to +2.0 V. So in these short circuit junction points, while there will be a very high current to flow, it is thought that the increase in the power consumed on the impedance, through the variable potential source, is not only met by the increase in the current, but also by the increase in the corrosion potential (I=V/R, P=V.I=V2/R, P; power-watt, V; volt, I; current, R; resistance). [41-44] Another effective factor in this regard is that the materials produced by additive manufacturing have a highly porous structure. Again, due to this porosity, the current can find a way to create a short circuit [40]. Thus, higher corrosion current, potential and rate were obtained in the untreated 316L sample compared to other coatings.

It can be seen that the ceramic coating samples had better corrosion behavior than the untreated sample. With the ceramic-based coating of the material, the service life of the material will increase. While there will be a loss of approximately 5.7 milliinches per year from the uncoated sample, it was seen from the results of the study that this loss would decrease to approximately 0.6 milliinches per year in the ceramic coated sample that this was the best result among to the type of ceramic coatings. In other words, only the coating part of the coated sample will give the loss in 1 year of the untreated sample in 9.5 years. This means that the material loss in 1 year due to corrosion in the untreated sample is approximately 10.5 years in the ceramic film-coated sample, which gives the best results. This means that ceramic coatings increase the service life of the material by about 10.5 years.

When the ceramic coatings are considered in themselves, the difference in current density, resistance, and corrosion rates is thought to be related to two factors. The first of these is the structural properties of the film such as the thickness, roughness, integrity, and chemical content [5, 6, 34, 45-51]. The more homogeneous and compact the coatings are on the surface, the less

deformation could be mentioned. It has been determined that the corrosion resistance is better in coatings that its film thickness is sufficiently high and the film integrity is preserved, which means, there are no cracks or little cracks than the others are in the coating film. However, in non-homogeneous and non-compact structures, if there are cracks and places where the film is thin, it is highly possible that the corrosion will start from these areas. Also, it is highly possible that the electrolyte will leak into the coating film and the corrosion will increase. The other factor of corrosion resistance was thought to be the electronegativity of the element atoms forming the ceramic structure on the surface [52-54]. It was known that as electronegativity between atoms increases, the ionic bonding increases. From the corrosion test results, it was seen that the film resistances were close to each other. But with a little difference, the cobalt oxide film had less film resistance. This was attributed that it was related to its film structure at the surface of the film and it was thought to be due to it having little cracks on the film surface. But, these cracks don't reach the substrate surface. So that the electrolyte can't influence the substrate surface. Also, it had a high interface resistance between the film and the substrate (Table 4.). So in the total system resistance of CoO was high and its corrosion rate was less. On the other hand, the lowest corrosion rate and current density were observed in $Ag_2O/CoO/TiO_2$, and the highest resistance value was observed in TiO_2 at the interface between the film and the substrate (Table 4.). TiO_2 had the highest electronegativity difference in these three ceramic structures, and it had the highest resistance. The lowest electronegativity belongs to Ag_2O, which has the lowest resistance and the highest current density and corrosion rate. While $Ag_2O/CoO/TiO_2$ composite coating had the lowest corrosion rate, current density, and highest film resistance, it was expected to show the highest resistance at the interface too. However, TiO_2 coating showed the highest resistance at the interface. Since Ag_2O is also present in the $Ag_2O/CoO/TiO_2$ coating, the Ag_2O structure will be damaged the most. Therefore, the resistance decreased. However, since there will be more resistant TiO_2 or CoO film layers under the damaged Ag_2O layer, it is thought that no damage has occurred in the lower resistant layers, which may have prevented the flow of current and caused less corrosion compared to other coatings. It was thought that the electronegativity of the coatings at the interface was very relevant to releasing the ions, because of fewer ionic bonds. Also, it had a rougher and less homogeneous film structure than the other coated films (Figure 2.). Because of this roughness and non-homogeneous structure, although the resistance of the film surface is high, the electrolyte influenced the film and reached the interface of the film and the substrate, and at the end, it reached the surface of the substrate. So that in the total system, it was seen that the Ag_2O was less stable and it had a higher corrosion rate than the other coatings.

The electrochemical impedance spectroscopy (EIS) method is a very useful method to determine the corrosion behavior and the detailed electrochemical process occurring on the surface. Figures 4-7 show the Nyquist and Bode curves of untreated and coated samples after the EIS scanning. The diameter of the graphical semicircles in the Nyquist plane represents the polarization resistance of the test samples, and the larger cycle indicates a lower corrosion rate. [5, 49, 55-57]. As can be seen from the Nyquist curves in Figure 4. the formation of a semi-circle with a lower radius of the untreated 316L compared to the ceramic-coated samples at low frequencies means that there is no protective layer on the surface of untreated 316L and that the corrosion resistance is low. It is seen from Figure 6. that the Nyquist curves of the ceramic-

coated samples are very close to each other. Also, they are in the way of forming a semi-circle to close, and while the diameters of these semi-circles increase the corrosion resistances increase too. It can be seen from the graph that the semicircular diameter of TiO_2 will be slightly higher than the others, and it can be said that the corrosion resistance is slightly higher than the others. It is known from the literature that, in Bode curves, the phase angle change in the low-frequency region shows the behavior of the metal; and the change of the phase angle in the high-frequency region, shows the strength of the film, and the size of the area under the Bode curves are related to the shielding efficiency of the film [58-62].

As seen in Bode curves (Figure 5. and 7), the uncoated 316L sample showed the lowest phase angle. Also, the least area under the Z_{mod}-frequency curve belongs to the uncoated 316L sample. The least phase angle and the lowest curve area meant poor corrosion behavior [56-58, 63-64]. Thus these results contributed to the worst corrosion behavior belonging to the uncoated 316L sample. In the phase angle-frequency curves in the low-frequency region, the phase angle, indicating the behavior of the metal, increased with TiO_2 and CoO ceramic coatings separately, while the phase angle in the high-frequency region, which indicated the surface film behavior, increased with Ag_2O ceramic-coating. This showed that the corrosion performance of ceramic coatings also varied according to the ceramic coating types. In Figure 7., it was seen that the areas under the Z_{mod}-frequency curves decreased rapidly with the increasing of the frequency, and they remained stable from mid-frequency to high frequencies. This meant that the ceramic coatings were resistant to corrosion behavior and protected the substrate material.

The equivalent circuit models for all samples and the obtained values of the circuit elements are shown in Figures 8, 9, and Table 4. The obtained simulated EIS fitting values were calculated with Gamry Echem Analyst software. The electronic components R_{sol}; the resistance of the electrolyte was simulated saliva fluid, R_{subs}; the charge transfer resistance in the interface, $C_{subs.}$; capacitance of the 316L substrate, R_{film}; the resistance of the ceramic film coatings, $Q_{subs.}$; the constant phase element (CPE) of the interface layer and substrate and $Q_{film.}$; the constant phase element (CPE) of the ceramic film coatings. Ceramic film coating resistance and charge transfer resistance are important parameters for evaluating the electrochemical behavior of the samples as mentioned in this section. Also, charge transfer resistance directly represents the corrosion rate in the interface between the layer and the substrate. It was seen from Table 4 that the EIS circuit fitting results supported the explanations about the corrosion behavior discussed in this section.

Table 4. EIS fitting parameters for uncoated and coated samples

					Q_{film}		Q_{subs}	
	$R_{sol.}$ ($\Omega.cm^2$)	R_{film} ($\Omega.cm^2$)	R_{subs} ($\Omega.cm^2$)	C_{subs} ($F.cm^{-2}$)	Y_0 ($\Omega.sec^n cm^{-2}$)	m $x10^{-3}$	Y_0 ($\Omega.sec^n cm^{-2}$)	n $x10^{-3}$
316L	217.1	93.62	-	$40.69x10^{-6}$	-	-	-	-
Ag_2O	348.7	156.5	$9.218x10^3$	-	$4.410x10^{-9}$	123.8	$2.151x10^{-3}$	768.2
CoO	352.4	120.6	$11.40x10^3$	-	$1.840x10^{-9}$	79.39	852.610^{-6}	786.3
TiO_2	442.0	149.7	$13.01x10^3$	-	$16.37x10^{-9}$	138.5	$726.5x10^{-6}$	749.4
$Ag_2O/CoO/TiO_2$	202.6	258.7	$8.569x10^3$	-	$48.35x10^{-9}$	134.9	$1.107x10^{-3}$	798.1

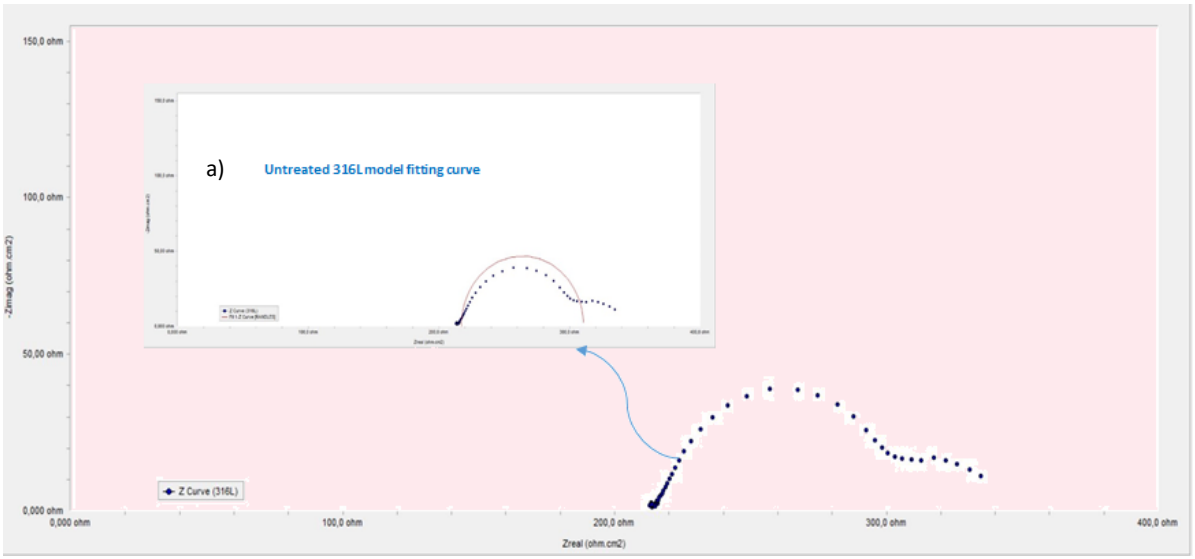

Figure 4. Nyquist curve of uncoated 316L sample a) model fit curve of uncoated 316L

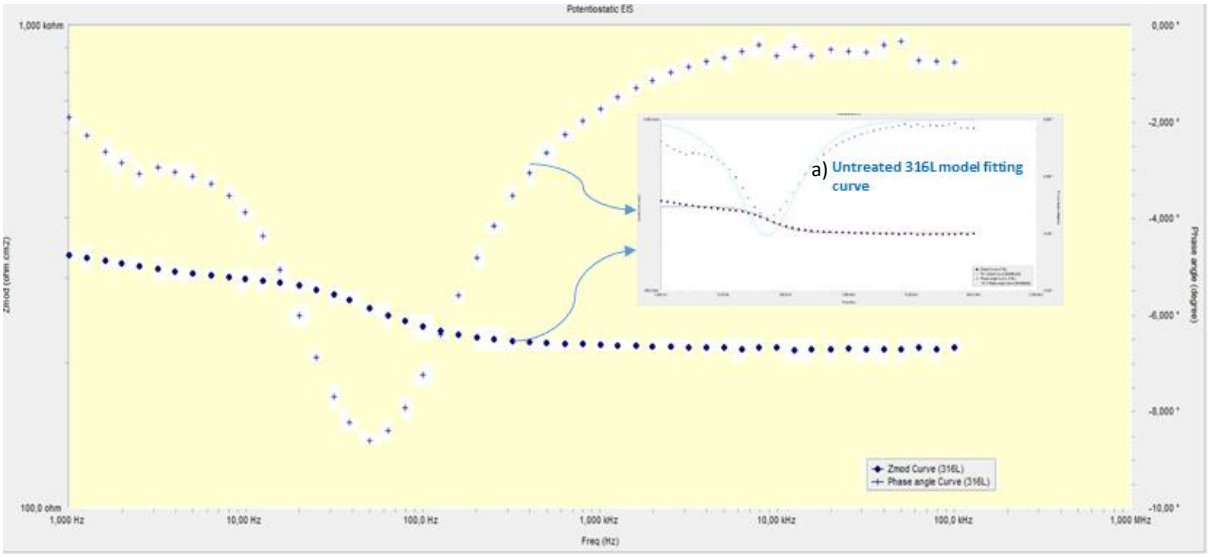

Figure 5. Bode curve of uncoated 316L sample a) model fit curves of uncoated 316L

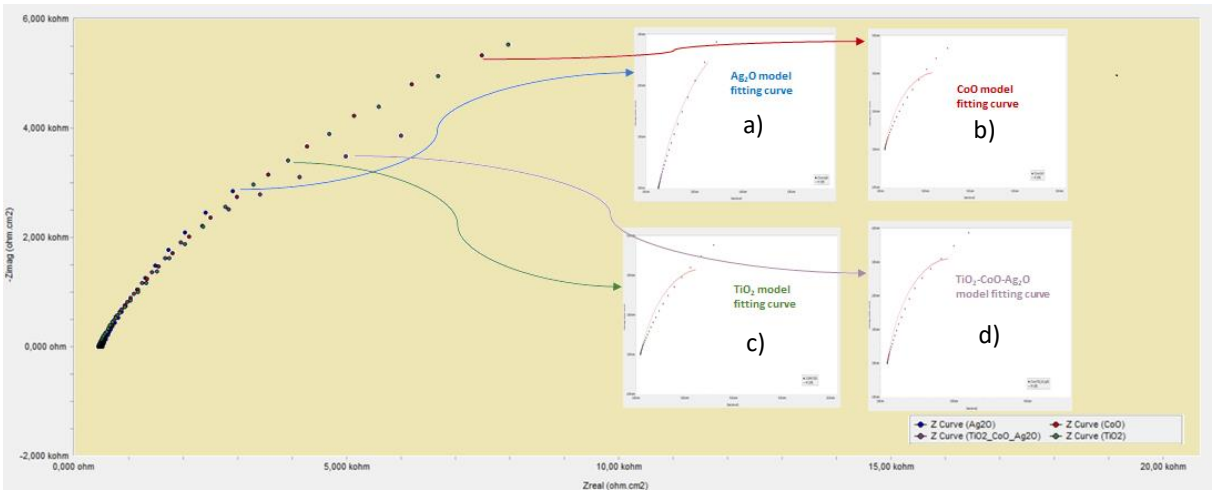

Figure 6. Nyquist curves of ceramic-coated samples a) model fit curve of Ag_2O ceramic-coating b) model fit curve of CoO ceramic-coating c) model fit curve of TiO_2 ceramic-coating d) model fit curve of TiO_2-CoO-Ag_2O ceramic-coating

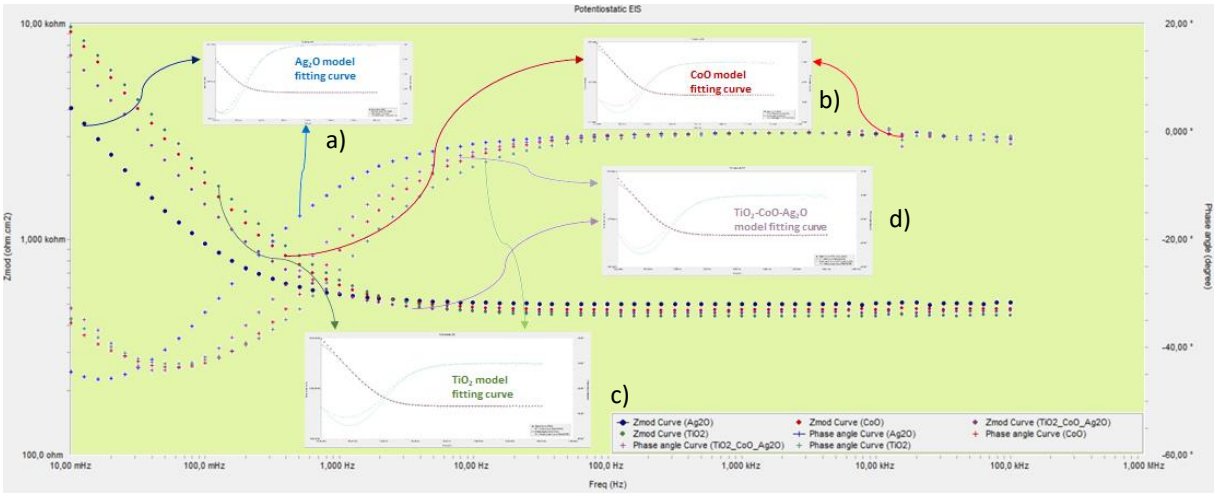

Figure 7. Bodet curves of ceramic-coated samples a) model fit curve of Ag_2O ceramic-coating b) model fit curve of CoO ceramic-coating c) model fit curve of TiO_2 ceramic-coating d) model fit curve of TiO_2-CoO-Ag_2O ceramic-coating

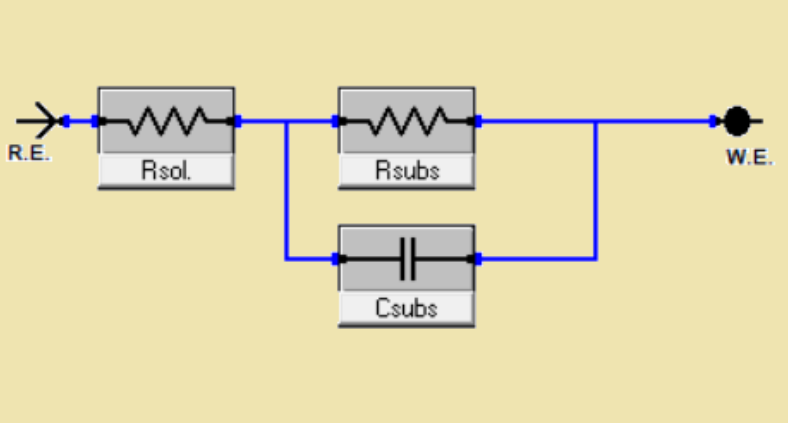

Figure 8. Equivalent circuit for (a) the uncoated 316L samples

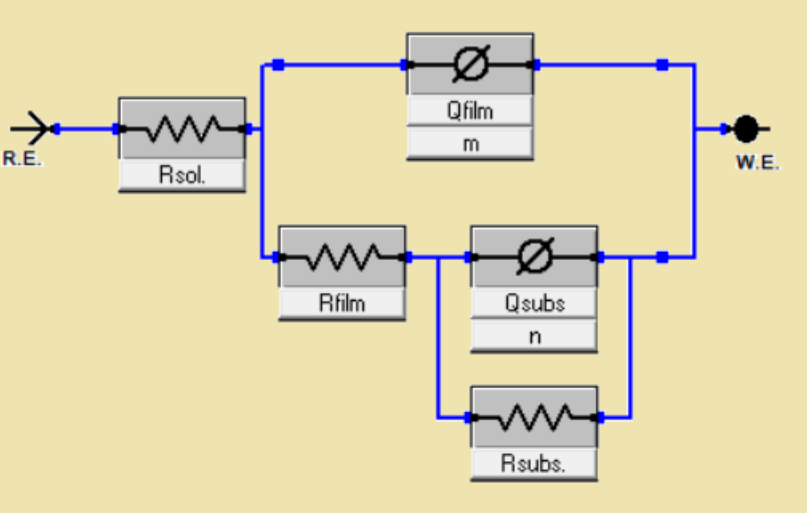

Figure 9. Equivalent circuit for the ceramic-coated samples.

4. Conclusion

In this study 316L stainless steel substrate was built by selective laser melting additive manufacturing method. To improve the corrosion behavior of 316L stainless steel, various ceramic film coatings were applied to the surface of the 316L. For this purpose Ag_2O, CoO, TiO_2, and the Ag_2O/CoO/ TiO_2 composite ceramic films were coated on the 316L sample surface by sol-gel dip-coating method. The structural and electrochemical properties of the coated ceramic films and the uncoated substrate were investigated. The following results were obtained;

- XRD analysis results showed that the different oxide coating processes occurred successfully on the substrate. 316L exhibited γ-austenite peaks (111) and (200) for uncoated samples and Ag_2O, CoO, and TiO_2 peaks were observed on the coated sample surfaces. Also, it was determined that TiO_2 oxide was rutile type according to the XRD peaks.
- Similar morphological features were observed in all coated samples from the SEM images. It was seen that the films were quite dense, non-colonic, non-porous, and compact, and a very thin and rough texture was formed on the surface of these films. However, it was observed that the quality of the surfaces of the films differed among themselves, depending on the fact that these properties were better.
- Potentiodynamic polarization and Electrochemical Impedance Spectroscopy (EIS) tests showed that the corrosion resistance of the ceramic film-coated samples displayed diversity with the various ceramic film coatings. But all ceramic film-coated samples had better corrosion behavior than the uncoated 316L sample. The uncoated 316L sample had the most corrosion rate among all the analyzed ceramic film-coated and uncoated samples.
- When the corrosion rates were compared, it was seen that the lowest corrosion rate belonged to the Ag_2O/CoO/ TiO_2 ceramic film-coated sample. According to the experiment results and the calculations it was seen that if this ceramic film coated on the 316L substrate surface, it would extend the service life of the substrate by approximately 10.5 years.
- The corrosion behavior of ceramic film-coated samples was compared to each other, and it was observed that Ag_2O showed the minimum corrosion resistance at the interface of the film and the substrate layer. But at the film surface, the minimum corrosion resistance was obtained at the CoO ceramic film-coated sample surface. These results were related to the electronegativity of the element atoms forming the ceramic film structures and also, the physical structure of the ceramic film surface.
- In the case of coated samples, the lowest corrosion rate was obtained at the Ag_2O/CoO/ TiO_2 ceramic composite film-coated sample, with both the dense, non-colonic, non-porous, and compact structure of the film and the positive effect of the electronegativity.

Ethics in Publishing

There are no ethical issues regarding the publication of this study.

References

[1] Yao, D., Liu, X., Wang, J., Fan, W., Li, M., Fu, H., Zhang, H., Yang, X., Zou, Q., An, X., (2021) Numerical insights on the spreading of practical 316 L stainless steel powder in SLM additive manufacturing, Powder Technology, *390*, 197-208.

[2] Wang, Y.F., Yu, C.F., Xing, L.L., Li, K.L., Chen J.H., Liu, W., Ma, J., Shen, Z.J., (2020) Grain structure and texture of the SLM single track, J. Mater. Process. Technol., *281*, 116591.

[3] Maconachie, T., Leary, M., Lozanovski, B., Zhang, X., Qian, M., Faruque, O., Brandt, M., (2019) SLM lattice structures: properties, performance, applications and challenges, Mater. Des., *183*, 108137.

[4] Samantaray, M., Thatoi, D.N., Sahoo, S., (2019) Modeling and optimization of process parameters for laser powder bed fusion of AlSi10Mg alloy, Lasers Manufact. Mater. Process., *6*, 356–373.

[5] Tekdir, H., Yetim, T., Yetim, A.F., (2021) Corrosion Properties of Ceramic-Based TiO_2 Films on Plasma Oxidized Ti6Al4V/316L Layered Implant Structured Manufactured by Selective Laser Melting, J Bionic Eng., *18*, 944–957.

[6] Tekdir, H., Yetim, A.F., (2021) Additive manufacturing of multiple layered materials (Ti6Al4V/316L) and improving their tribological properties with glow discharge surface modification, Vacuum, *184*, 109893.

[7] Yetim, A. F., Yazici, M., (2014) Wear resistance and non-magnetic layer formation on 316L implant material with plasma nitriding, J. Bionic Eng., *11 (4)*, 620-629.

[8] Obadele, B.A., Andrews, A., Olubambi, P.A., Mathew, M.T., Pityana, S., (2015) Effect of ZrO_2 addition on the dry sliding wear behavior of laser clad Ti6Al4V alloy, Wear, *328 (329)*, 295-300.

[9] Fernandes, A.C., (2006) Tribocorrosion behavior of plasma nitrided and plasma nitrided + oxidised Ti6Al4V alloy, Surf. Coating. Technol., *200 (22)*, 6218-6224.

[10] Zhu, Y., Zou, J., Yang, H., (2018) Wear performance of metal parts fabricated by selective laser melting: a literature review, J. Zhejiang Univ. A, *19(2)*, 95-110.

[11] Sing, S.L., Yeong, W.Y., Wiria, F.E., (2016) Selective laser melting of titanium alloy with 50wt% tantalum: microstructure and mechanical properties, J. Alloys Compd., *660*, 461-470.

[12] Song, C., Zhang, M., Yang, Y., Wang, D., Jia-kuo, Y., (2018) Morphology and properties of CoCrMo parts fabricated by selective laser melting, Mater. Sci. Eng. A, *713*, 206-213.

[13] Simson, T., Emmel, A., Dwars, A., Böhm, J., (2017) Residual stres measurements on AISI 316L samples manufactured by selective laser melting, Addit. Manuf., *17*, 183-189.

[14] Mohammed, M.T., (2018) Mechanical properties of SLM-Titanium materials for biomedical applications: a review, Mater. Today Proc., *5 (9)*, 17906-17913.

[15] Agopovichev, A.V., Kokareva, V.V., Smelov, V.G., Sotov, A.V., (2016) Selective laser melting of titanium alloy: investigation of mechanical properties and microstructure, IOP Conf. Ser. Mater. Sci. Eng., *156* (1).

[16] Čapek, J., Machová, M., Fousová, M., Kubásek, J., Vojtěch, D., Fojt, J., Jablonská, E., Lipov, J., Ruml, T., (2016) Highly porous, low elastic modulus 316L stainless steel scaffold prepared by selective laser melting Materials Science and Engineering C, *69*, 631-639.

[17] Bremen, S., Meiners, W., Diatlov, A., (2012) Laser. Technik. J., *9*, 33–38.

[18] Kruth,J.,Froyen,P.,Van,L.,Vaerenbergh,J.,(2004)J.Mater. Process.Technol.,*149*, 616–622.

[19] Laohaprapanon, A., Jeamwatthanachai, P., (2012) Wongcumchang, M., et al., Mater. Manuf. Technol. II Pts 1 and 2, 816–820.

[20] Cherry, J.A.,Davies,H.M., Mehmood, S.,(2014) Int. J. Adv. Manuf. Technol.,*76*, 869–879.

[21] Yadroitsev,I.,Krakhmalev,P.,Yadroitsava,I.,(2013)J.Mater.Process.Technol.*213*,606–613.

[22] Li, R., Shi, Y., Wang, Z., (2010) Densification behavior of gas and water atomized 316L stainless steel powder during selective laser melting Appl. Surf. Sci., *256*, 4350–4356.

[23] Li, R., Liu, J., Shi, Y., (2012) Int. J. Adv. Manuf. Technol., *59*, 1025–1035.

[24] Tekdir, H., Yetim, T., Yetim, A.F., (2021) Corrosion Properties of Ceramic-Based TiO_2 Films on Plasma Oxidized Ti6Al4V/316L Layered Implant Structured Manufactured by Selective Laser Melting, J Bionic Eng, *18*, 944–957.

[25] Bloyce, A., Qi, P.Y., Dong, H., Bell, T., (1998) Surface modification of titanium alloys for combined improvements in corrosion and wear resistance. Surface and Coatings Technology, *107*, 125–132.

[26] Bolzoni, L., Meléndez, I. M., Ruiz-Navas, E.M., Gordo, E., (2012) Microstructural evolution and mechanical properties of the Ti-6Al-4V alloy produced by vacuum hot-pressing. Materials Science and Engineering A, *546*, 189–197.

[27] Wu, G., Zhang, S., Wang, Y., Sun, M., Zhang, Q., Kovalenko, V., Yao, J., (2022) Porous ceramic coating formed on 316L by laser cladding combined plasma electrolytic oxidation for biomedical application, Trans. Nonferrous Met. Soc. China, *32*, 2993−3004.

[28] Yang, Z., Tu, Q., Maitz, M.F., Zhou, S., Wang, J., Huang, N., (2012) Direct thrombin inhibitorbivalirudin functionalized plasma polymerized allylamine coating for improved biocompatibility of vascular devices, Biomaterials, *33*, 7959−7971.

[29] Katta, P., Nalliyan, R., (2019) Corrosion resistance with selfhealing behavior and biocompatibility of Ce incorporated niobium oxide coated 316L SS for orthopedic applications, Surface and Coatings Technology, *375*, 715−726.

[30] Garcia-Lobato, M.A., Mtz-Enrıquez, A. I., Garcia, C.R., Velazquez-Manzanares, M., Avalosbelmontes, F., Ramos-Gonzalez, R., Garciacerda, L.A., (2019) Corrosion resistance and in vitro bioactivity of dense and porous titania coatings deposited on 316L SS by spraying method, Applied Surface Science, *484*, 975−980.

[31] Moshref-Javadi, M., Edris, H., Shafyei, A., Salimi-Jazi H., Abdolvand, E., (2018) Evaluation of hydrogen permeation through standalone thermally sprayed coatings of AISI 316L stainless steel, International Journal of Hydrogen Energy, *43*, 4657−4670.

[32] Ke-Dong, Z., Jian-Xin, D., Shu-Ting, L., Xiao-Ming, Y., (2016) Effect of micro/nano-textures and burnished MoS2 addition on the tribological properties of PVD TiAlN coatings against AISI 316 stainless steel, Surface and Coatings Technology, *291*, 382−395.

[33] Shu-Wei, G., Dong-Hai, X., Yu, L., Yan-Meng, G., Yan-Hui, L., (2020) Corrosion characterization of ZrO_2 and TiO_2 ceramic coatings via air plasma spraying on 316 stainless steel in oxygenated sub- and supercritical water, The Journal of Supercritical Fluids, *157*, 104716.

[34] Çomaklı, O., Yazıcı, M., Kovacı, H., Yetim, T., Yetim, A.F., Çelik, A., (2018) Tribological and electrochemical properties of TiO_2 films produced on Cp-Ti by sol-gel and SILAR in bio-simulated environment, Surf. Coat. Technol., *352*, 513-521.

[35] Banerjee, D.A., Kessman, A.J., Cairns, D.R., Sierros, K.A., (2014) Tribology of silica nano-particle-reinforced, hydrophobic sol–gel composite coatings, Surf. Coat. Technol., *260*, 214–219.

[36] Mora, L.V., Naik, S., Paul, S., Dawson, R., Neville, A., Barker, R., (2017) Influence of silica nanoparticles on corrosion resistance of sol-gel based coatings on mild steel, Surf. Coat. Technol., *324*, 368–375.

[37] Çomakli, O., Yazici, M., Yetim, T., Yetim, A.F., Çelik, A., (2017) The effects of aging time on the structural and electrochemical properties of composite coatings on CP-Ti substrate, J. Bionic Eng., *14*, 532–539.

[38] Margareth, R.C., Marques, Loebenberg, R., Almukainzi, M., (2011) Simulated Biological Fluids with Possible Application in Dissolution Testing Dissolution Technologies, August doi.org/10.14227/DT180311P15.

[39] Duffo, G.S., Castillo E.Q., (2004) Development of an artificial saliva solution for studying the corrosion behavior of dental alloys. Corrosion, *6*, 594–602.

[40] Pathak, S., Böhm, M., Kaufman, J., Kopeček, J., Zulić, S., Stránský, O., Shukla, A., Brajer, J., Beránek, L., Radhakrisnan, J., Rostohar, D., Mocek, T., (2023) Surface integrity of SLM manufactured meso-size gears in laser shock peening without coating, Journal of Manufacturing Processes, *85*, 764-773.

[41] Arturo, G.R.M., Hugo, L.M.V., Rafael, G.H., Egberto, B.B., Antonio, G.S.J., (2015) Electrochemical Characterization of AISI 2205 Duplex Stainless Steel Welded Joints with Electromagnetic Interaction, Procedia Materials Science, *8,* 950-958.

[42] Gomes de Souza, D.D.B., Vilarinho, L.O., (2020) Influence of present phases in corrosion and mechanical behavior of UNS S31803 duplex stainless steel welded by conventional short circuit MIG/MAG process, Journal of Materials Research and Technology, *9,* 11244-11254.

[43] Araneda, A.A.B., Kappes, M.A., Rodríguez, M.A., Carranza, R.M., (2022) Pitting corrosion of Ni-Cr-Fe alloys at open circuit potential in chloride plus thiosulfate solutions, Corrosion Science, *198,* 110121.

[44] Wasekar, N.P., (2022) The influence of grain size and triple junctions on corrosion behavior of nanocrystalline Ni and Ni-W alloy, Scripta Materialia, *213*, 114604

[45] Yetim, T., Turalioglu, K., Taftali, M., Tekdir, H., Kovaci, H., Yetim, A.F., (2022) Synthesis and characterization of wear and corrosion resistant Ni-doped Al_2O_3 nanocomposite ceramic coatings by sol-gel method, Surf. Coat. Technol., *444*, 128659.

[46] Çelik, A., Acar, M.T., Yetim, T., Kovacı, H., Yetim, A.F., (2020) Improving structural, tribological and electrochemical properties of Ti6Al4V alloy with B-doped TiO_2 thin films, Tribology International, *146*, 106210.

[47] Çeliker, M., (2019) Conicraly Bağ ve Ysz İçerikli Termal Bariyer Kaplamaların Elektrokimyasal Korozyon Davranışlarının İncelenmesi, Yüksek Lisans Tezi, Bartın.

[48] Doğru, B. M., Yazıcı, B., (October, 06-09-2010)135 Poli(Pirol-Ko-O-Anisdin) Kaplı Alüminyumun %3,5 NaCl'deki Korozyon Davranışı, XII. International Corrosion Symposium, Eskişehir, Turkey.

[49] Bozkurt, Y.B., Çelik, A., (2022) Tailoring biodegration rate of AZ31 magnesium alloy Electrochimica Acta, *435*, 141403.

[50] Jihui, D.Z., Hu, W.W., (2022) Hydroxyapatite film prepared by hydrothermal method on layered double hydroxides coated Mg Alloy and its corrosion resistance, Colloids and Surfaces A: Physicochemical and Engineering Aspects, *647*, 129075.

[51] Husien, V., Haakmann, S.F., Brinkbaumer, J., Ulbricht, M., (2022) Comparison of the nucleation and growth of a phosphate conversion coating on Zn–Al and Zn–Al–Mg coatings under the influence of a corrosion inhibitor film, Surface & Coatings Technology, *451*, 129044.

[52] Wang, Y., Si, J., Si, Y., Shi, Z., (2023) Preparation and electrochemical corrosion performances of Zr-Ti-Ni-Cu-Be high-entropy bulk metallic glasses, Materials Science & Engineering B, *289*, 116267.

[53] Hernandez, R., Alma, B., Jose, D.M., Juan, G.P., Jose, M.O., Domínguez, M.E., Mujica, V., (2022) Experimental and theoretical study on the effectiveness of ionic liquids as corrosion inhibitors, Computational and Theoretical Chemistry, *1210*, 113640.

[54] Dong Wei, B., Tianyi, L., Longjun, Z., Yueming, C., Yonggang, F., Hai, Z., Weijian, L., Sun, Y.Y., (2023) Clarifying the effect of a small amount of Cr content on the corrosion of Ni-Mo steel in tropical marine atmospheric environment, Corrosion Science, *210*, 110813.

[55] Turalioglu, K., Taftalı, M., Tekdir, H., Çomaklı, O., Yazıcı, M., Yetim, T., Yetim, A.F., (2021) The tribological and corrosion properties of anodized Ti6Al4V/316L bimetallic structures manufactured by additive manufacturing, Surf. Coat. Technol., *405*, 126635.

[56] Manazoğlu, M., (2013) Elektrokimyasal Yöntemle Nikelmolibden Alaşım Kaplamaların Üretimi ve Karakterizasyonu, Yüksek Lisans Tezi İstanbul.

[57] Küstü, C., (2008) Asitli Ortamdaki Korozyona Karşı Schıff Bazı Temelli Bazı Yeni İnhibitörlerin Geliştirilmesi, Yüksek Lisans Tezi.

[58] Duran, B., Çakmakcı, İ., Bereket, G., (06-09-2010) Bakır Üzerinde Pirol Ve N-Metil Pirolün Kopolimeri İle Çift Kaplamalarının Sentezi ve Korozyon Performanslarının Araştırılması, XII. International Corrosion Symposium, Eskişehir, Turkey.

[59] Akbarinezhad, E., Faridi, H.R., (2008) Surface Engineering, *24*, 280-286.

[60] Zhao, X., Wang, J., Wang, Y., Kong, T., Zhong, L. And Zhang, W., (2007) Electrochemistry Communications, *9*, 1394-1399.

[61] Hırayama, R. and Haruyama, S., (1991) Electrochemical Impedance for Degraded Coated Steel Having Pores, Corrosion, *47*, 952-958.

[62] Akbarinezhad, E., Bahremandi, M., Faridi, H.R., Rezaei, F., (1988) Another approach for ranking and evaluating organic paint coatings via electrochemical impedance spectroscopy, Corrosion Science, *51*, 356-363, 2009. 24.

[63] Çoban, K., (2006) Ketonik Bazlı Reçinelerle Paslanmaz Çelik ve Bakırın Korozyonunun Önlenmesi, Yüksek Lisans Tezi.

[64] Mutlu, R.N., Ateş, S., Mert, B.D., Yazıcı, B., (15-17 Ekim 2014) Sodyum Molibdat (Na_2MoO_4) Katkısının, 7075 Aluminyum Alaşımının Sülfürik Asit İçerisindeki Eloksal İşlemine ve Korozyon Davranışlarına Etkisi, 13. Uluslararası Korozyon Sempozyumu Bildiriler Kitabı, Fırat Üniversitesi, Elazığ, Türkiye.